

DISTRIBUTED AND NON-STEADY-STATE MODEL OF AN AIR COOLER

Ricardo Nicolau Nassar Koury

Universidade Federal de Minas Gerais, Av. Antônio Carlos, 6627, Pampulha, Belo Horizonte, Brasil
koury@demec.ufmg.br

Luiz Flávio Neves de Castro

Universidade Federal de Minas Gerais
lfncastro@hotmail.com

Luiz Machado

Universidade Federal de Minas Gerais
luzm@demec.ufmg.br

Abstract. *The purpose of this work is to develop a numerical model of an air cooler, which is commonly found in air-conditioning applications. The model divides the air cooler in control volumes in which mass, energy and momentum balance equations are applied and solved. The fourth order Runge-Kutta method is used to solve the refrigerant equations and the Finite Differences method is applied to solve the air and tube wall equations. The model presented is able to simulate different geometries of air coolers and also to work with several refrigerants. Theoretical data obtained by model simulations working with R22 and R410a refrigerants, repeated tendencies observed in experimental data taken from literature. Model response to a system start up and also to mass flow rate changes at the air cooler inlet and outlet working with R22 is presented.*

Keywords. *Air cooler, Refrigeration, Numerical model, Non-steady-state*

1. Introduction

The evaporator is responsible for the heat transfer from a low-temperature region to a refrigerant that evaporates and superheats in its tubes. The air coolers are one of the most common kinds of evaporators. They are characterized by the use of air as secondary working fluid. These heat exchangers are widely used in the HVAC&R industry.

The study of air coolers is complicated by several reasons. Firstly, the refrigerant is flowing under phase changing conditions inside the tubes, which results in significant variations of heat transfer coefficients and flow characteristics along the tubes. Secondly, the presence of water vapor in the air results in simultaneous heat and mass transfer between the air and the tubes. Moreover, the complexity of the airflow along the finned tubes is high. Finally, in order to evaluate the values of heat and mass transfer coefficients, it is necessary to use semi-empirical correlations, which still being discussed in literature.

The purpose of this work is to develop a numerical model to simulate the behavior of an air cooler operating under dynamic conditions.

2. Literature review of numerical models

The numerical models found in literature, when considering the operation conditions of the system, can be classified under two wide categories: steady state and non-steady-state or dynamic models. The purpose of the study determines the kind of model to be adopted. Usually, the steady-state models are used to study new refrigerants in order to substitute that contribute to the ozone layer depletion. They are also used in the design and optimization of refrigeration and heating systems by vapor compression. The dynamic models are adopted to control the superheating degree in evaporators outlet, and also to study instabilities of the pair evaporator-thermostatic expansion valve, among other applications.

The models can also be classified under two categories depending on the need of experimental data: black box and deductive models. The black box models are developed in two different parts. First of all, a mathematical expression that relates the evaporator inlet with outlet unknowns is derived. After that, experimental data is used to provide the parameters of the expression. Since the parameters are obtained through experimental data, the black box models reproduce precisely the phenomenon. However, as these models do not take into account the physical laws that describe the evaporator behavior, its application is restrict to the experimental working range. The deductive models are based on the application of the physics laws of energy, mass and momentum conservation to the studied system. They are classified in global models and discretized models.

The global models, as shown by its own name, consider the evaporator globally. Thus, temperature, quality, void fraction, and density of the refrigerant, as well as the temperatures of secondary fluid and tube walls are represented by mean values. The heat transfer coefficients between the fluids and the tube walls are considered constant along the entire heat exchanger. This kind of model is suitable to shell and tube evaporators.

The discretized or "multizone" models divide the heat exchanger in several control volumes. The mass, momentum, and energy balance equations are solved in each control volume, and the heat transfer coefficients, pressure losses and void fraction in the boiling region are locally obtained through correlations taken from literature. This is the most appropriated kind of model to air coolers.

MacArthur and Grald, (1989) presented a deductive multizone model to study an air-air heat pump operating under dynamic conditions. In this model, the evaporator and the condenser are divided in control volumes and the energy, mass, and momentum balance equations are applied and solved in each of them. In the last control volume, the outlet mass flow rate of refrigerant must be equal to that gave by the compressor model. If these two values are not coincident, the saturation temperature is then changed. The procedure is repeated until the two mass flow rates converge. The changing of ebullition to superheating region is made when the outlet enthalpy of a control volume is equal to the saturated vapor enthalpy. The authors also noticed that the dynamic response of the model is highly influenced by the chosen void fraction correlation. The correlation proposed by Zivi was chosen among those tested.

Wang and Toubert, (1991) proposed a deductive model to study the dynamic behavior of an air cooler. They describe the mass transport in a evaporator using a void fraction propagation equation. For that, it is assumed that the slip effect between the liquid and vapor phases in the two-phase flow is a steady phenomenon. In order to calculate the void fraction from the vapor quality, the PHOENICS software is used to solve the steady-state momentum equation. The local rate of evaporation is calculated through the mass balance equation applied to the vapor (or liquid) phase. The position where the void fraction becomes zero corresponds to the transition from ebullition to superheating region. Since this position is known, the length of ebullition is obtained. From this value, the saturation temperature is calculated through an expression derived from the mass and energy balance equations. With the new saturation temperature, the length of the ebullition region is recalculated, and the operations are repeated until the length (or the saturation temperature) converges.

It is important to say that Wang and Toubert consider the humid air as the secondary fluid. As the air temperature and absolute humidity are unknowns, concentration and energy equations are derived. The authors also take into account the heat transfer by conduction along the fins between the adjacent control volumes. Experimental data showed the accuracy of the model.

Jia et al, (1995) presented a deductive multizone model to simulate the dynamic behavior of an air cooler. The model is simplified since the saturation pressure is imposed. The numerical simulations are made to steps applied to the mass flow rate in the evaporator inlet. The superheating and the air temperature are the analyzed responses.

Machado, (1996) developed a deductive multizone model to study the dynamic behavior of a coaxial 3-tube evaporator, which used water as secondary fluid. In this evaporator, refrigerant flows inside the internal tubes, while water flows counter-current through the space between the internal and external tubes. In this model, the refrigerant equations are solved separated from the tube walls and water equations. From an initial guess to the profile of tube walls temperature, the equations related to the refrigerant are solved by fourth-order Runge-Kutta algorithm. Then, the water and tube walls temperature profiles are obtained through the implicit finite-difference method. These calculations are repeated until the tube wall profile calculated is equal to the initial guess of the specific iteration. The model algorithm is presented in a very detailed form and an experimental study showed its accuracy.

Liang et al, (2001) developed a deductive multizone model to analyze the performance of complex refrigerant circuitry of evaporator coils. In this model, the refrigerant inlet enthalpy is given by an assumed condenser outlet condition. An outlet temperature and an outlet pressure corresponding to a saturation temperature specify the refrigerant outlet state. For a given mass flow rate, the refrigerant inlet temperature and the coil length are iterated until the refrigerant outlet enthalpy and pressure converge. The authors presented a comparative study between experimental data to different configurations of tubes in the same evaporator e theoretical data obtained through model simulations. Once the model was validated, a new series of simulations was done with different tube circuitry in an evaporator coil in order to verify the effects of these circuitries in the equipment performance. It was verified that compared with a common coil, using complex refrigerant circuitry arrangement where the refrigerant circuits are properly branched or joined may reduce the heat transfer are by around 5% in coil design.

3. The air coil numerical model

There are many different tube circuitry arrangements for an air cooler. Thus, it is important to develop a model that is able to work with several kinds of geometries of evaporator coils. In this model, the air coil geometry (the position and the quantity of tubes as well as the flow direction in these tubes) is given to the main program by an input file. Therefore, it is possible to study different refrigerant circuitry arrangements with the model changing only a few parameters in the input file.

The air coil studied in this paper is composed by three rows of eight finned refrigerant tubes. The secondary fluid (humid air) flows in a forced cross-flow. The air coil is made of copper tubes with plan aluminum fins and inner and outer tubes diameters are, respectively, 9mm and 10mm. The fin linear density is 277 fins/m and their width is 0,3mm. Length, height and depth of the evaporator are, respectively, 300mm, 200mm and 60mm. A lateral view of the evaporator, where the refrigerant path is represented, is presented in Fig (1).

Among the different kinds of models presented in section 2, it was chosen a deductive multizone model similar to that presented by MacArthur, (1989). So that, the evaporator is divided in a number of control volumes and the mass, energy and momentum balance equations are applied to refrigerant, secondary fluid and tube walls. The heat and mass transfer coefficients; the friction pressure losses and the void fraction are obtained through literature correlations. The approach presented by Machado, (1996) was chosen to solve the differential equations system.

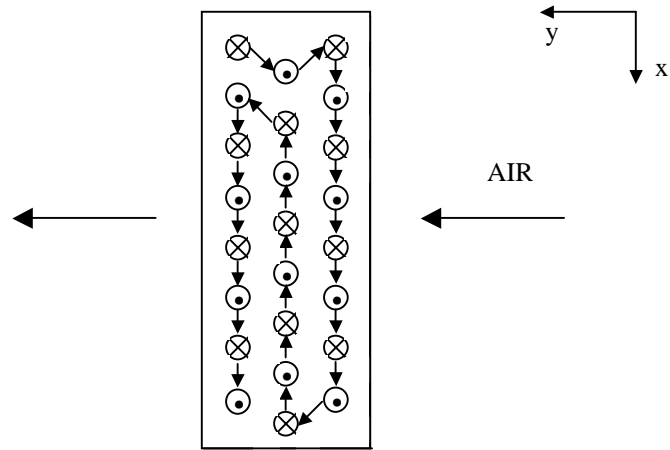


Figure 1. Refrigerant path along the air cooler.

3.1. Numerical model assumptions

The developed model considered the following assumptions:

- 1) The refrigerant, air and tube walls properties are considered equal along each volume cross-section.
- 2) Air and refrigerant flow are one-dimensional.
- 3) The vapor and liquid phases are in equilibrium along the ebullition region.
- 4) The axial conduction and the radial temperature gradient along the tube walls are ignored.
- 5) The thermal losses of the evaporator are ignored.
- 6) The thermal and pressure losses along the branches are ignored.
- 7) The air heat transfer coefficient is uniform.
- 8) The fin temperature is considered equal to the tube wall temperature. In order to minimize this error, a fin efficiency η_{fin} is adopted.
- 9) The airside heat and mass transfers between adjacent control volumes are ignored.
- 10) There is no ice formation in the external tube walls.

3.2. Numerical model inputs and outputs

As it was said before, the numerical model is composed by a differential equations system. Thus, a group of initial and boundary conditions is necessary to solve this system. The initial conditions correspond to the values, taken at the initial instant $t = 0$, of the equations system unknowns along the evaporator. They are the spatial profile of pressure, temperature and mass flow rate of refrigerant, air and tube walls temperatures, and air humidity. The boundary conditions correspond to the values of the inputs at every time step. They are the inlet and outlet refrigerant mass flow rate, the refrigerant inlet enthalpy, the air mass flow rate and the air inlet temperature and humidity.

The resolution of the differential equations system will give the spatial profiles of refrigerant, tube walls and air temperatures, and air humidity. It will also give the inlet and outlet refrigerant temperature and outlet air humidity and temperature. These are the output of the model. The Fig (2) shows a block diagram of the numerical model.

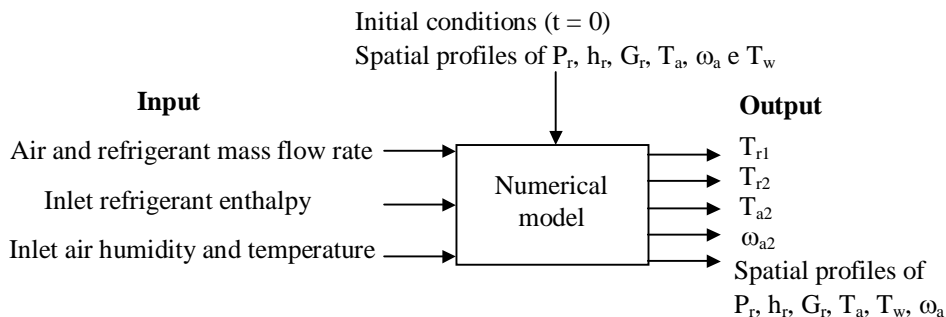


Figure 2. Block diagram of the numerical model

3.3. Numerical model equations

The numerical model is derived through the application of the mass and energy balance equations to the air, mass, energy and momentum balance equations to the refrigerant and energy balance equation to the tube wall, in every cross-section of the evaporator. Since the resolution of this equations system is complicated, the approach proposed by

Machado, (1996) was chosen to solve it. In this method, the refrigerant, air and tube walls equations are solved separately. In every equation the temporal derivatives were substituted by differentials, while the spatial derivatives were represented in explicit form. Thus, the Eq. (1) to (3) represent the equations system to the refrigerant.

$$\frac{\partial h_r}{\partial z} = \frac{1}{G_r} \left[\frac{P_r - P_r^0}{\Delta t} - \frac{h_r - h_r^0}{\Delta t} \rho_r + \alpha_r \frac{p_r}{A_r} (T_w - T_r) \right] \quad (1)$$

$$\frac{\partial G_r}{\partial z} = - \left(\frac{\rho_r - \rho_r^0}{\Delta t} \right) \quad (2)$$

$$\frac{\partial \bar{P}_r}{\partial z} = - \left(\frac{G_r - G_r^0}{\Delta t} \right) - \left(\frac{dP}{dz} \right)_r \quad (3)$$

Where G represents the mass velocities, h, P, ρ , and T represent, respectively, the enthalpies, the pressures, the densities, and the temperatures, while p_r is the wet perimeter, and Δt is the time step. The subscript 0 refers to the anterior iteration.

From an initial guess to the saturation pressure P_{r1} and from the known values of inlet refrigerant enthalpy and mass flow rate, it is possible to calculate the inlet \bar{P}_r at the first control volume (refrigerant inlet). From the known values, in the center of each control volume, of P_r , h_r , ρ_r e G_r , the values of outlet h_r , G_r and \bar{P}_r are obtained through fourth-order Runge-Kutta algorithm. These values are assumed to be the inlet values of the next element. The ebullition to superheating region transition is made by the comparison between the outlet refrigerant enthalpy h_r at each element and the saturated vapor enthalpy h_f . For two-phase flow and superheating regions, the value of the heat transfer coefficient α_r is taken at the control volume inlet. This coefficient, as well as the void fraction, is calculated using local correlations taken from literature. The two-phase region temperature is calculated in each control volume from the saturation pressure through the equation. The mass is determined through the void fraction and a saturated refrigerant state equation. A state equation is also used to the superheated vapor. The refrigerant properties are obtained through equations proposed by Cleland, (1986).

In the last control volume outlet, the value of G_r must be equal to the mass flow rate imposed by the compressor. If these two values are not identical, another value of P_{r1} , determined by the Newton-Raphson algorithm, is assumed. The iterations are repeated until the mass flow rates are equal.

Since the humid air is the secondary fluid, there are two different situations to the tubes and air heat exchange. First, if the tube walls temperature is greater than the dewpoint temperature, so that there is no condensation of water vapor along the tube walls and, second, if the opposite occurs, so that there is a simultaneous heat and mass transfer. The air energy equation, however, is the same to both cases. This is possible because the mass balance equation for the water vapor present in the air, depending on the situation, makes the condensation terms equal zero in energy equation.

Besides the question of existence or not of water vapor condensation, the division of the air cooler airside in control volumes is complicated because of its geometry. The Fig (3) shows the two different kinds of control volumes used in the model. The difference between them is given by the presence of the tube. Thus, in the control volumes without tube, the heat transfer from tube to refrigerant term is eliminated from the equation, and different air passage and heat transfer surface areas are adopted.

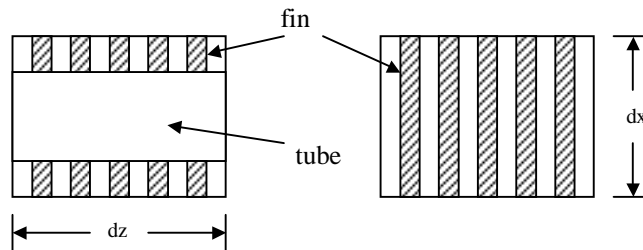


Figure 3. Two different kinds of control volumes – airside

The Eq. (4) and (5) are obtained through application of energy balance equation to the air and the tube walls.

$$\left[\dot{m}_{ha} c_v \frac{1}{\Delta t} + 2c_{pa} + \alpha_a (A_w + \eta_{fin} A_{fin}) + 2a_1 \right] \cdot T_a - \alpha_a (A_a + \eta_{fin} A_{fin}) \cdot T_w = \dot{m}_{ha} c_v \frac{1}{\Delta t} T_a^0 + 2c_{pa} T_{a1} + \omega_1 h_{v1} - \omega_2 (a_0 - a_1 T_{a1}) - (\omega_1 - \omega_2) h_{12} \quad (4)$$

$$\alpha_a (A_w + \eta_{fin} A_{fin}) \cdot T_a + \left[\rho_w A_w c_{pw} \frac{1}{\Delta t} + \alpha_a (A_w + \eta_{fin} A_{fin}) + \alpha_r A_r + \sum \frac{\lambda_{ij} A_{ij}}{\Delta L_{ij}} \right] \cdot T_w = \alpha_r A_r T_r + \sum \frac{\lambda_{ij} A_{ij}}{\Delta L_{ij}} \cdot T_w^{ij} \quad (5)$$

Where A represents the areas, c_v is the specific heat at constant volume, $\sum \frac{\lambda_{ij} A_{ij}}{\Delta L_{ij}}$ corresponds to the sum of the terms related to the heat conduction from adjacent volumes, T_w^{ij} corresponds to the tube walls temperatures of these control volumes, and a_1 and a_0 are coefficients of a linear regression to estimate the outlet water vapor enthalpy. The fin efficiency, η_{fin} , is given by Eq (6) (Wang and Touber, 1991).

$$\eta_{fin} = \frac{\text{tgh}\left\{0,5 \cdot (\Delta z_i - D) \cdot [2\psi\alpha_a (\lambda_{fin} y)]^{0,5}\right\}}{0,5 \cdot (\Delta z_i - D) \cdot [2\psi\alpha_a (\lambda_{fin} y)]^{0,5}} \quad (6)$$

Where Δz_i is the distance between tube centers in x-axis, D is the external diameter of the tube, y is the fin width, α_a is the air heat transfer coefficient, λ_{fin} is the fin thermal conductivity and ψ is equal 0,85 to cylindrical basis fins (Wang and Touber, 1991).

In order to solve the system composed by the Eq (4) and (5), it is necessary to obtain the outlet absolute air humidity, ω_2 . The flow rate of condensate liquid is obtained from Eq (7).

$$\dot{m}_{l2} = \dot{m}_a (\omega_1 - \omega_2) = \alpha_m (A_w + \eta_{fin} A_{fin}) (\omega_a - \omega_w) \quad (7)$$

Thus, considering that ω_a is the average between ω_1 e ω_2 , ω_2 can be written like Eq. (8).

$$\omega_2 = \frac{[2\dot{m}_a - \alpha_m (A_w + \eta_{fin} A_{fin})] \cdot \omega_1 + 2\alpha_m (A_w + \eta_{fin} A_{fin}) \cdot \omega_w}{\alpha_m (A_w + \eta_{fin} A_{fin}) + 2\dot{m}_a} \quad (8)$$

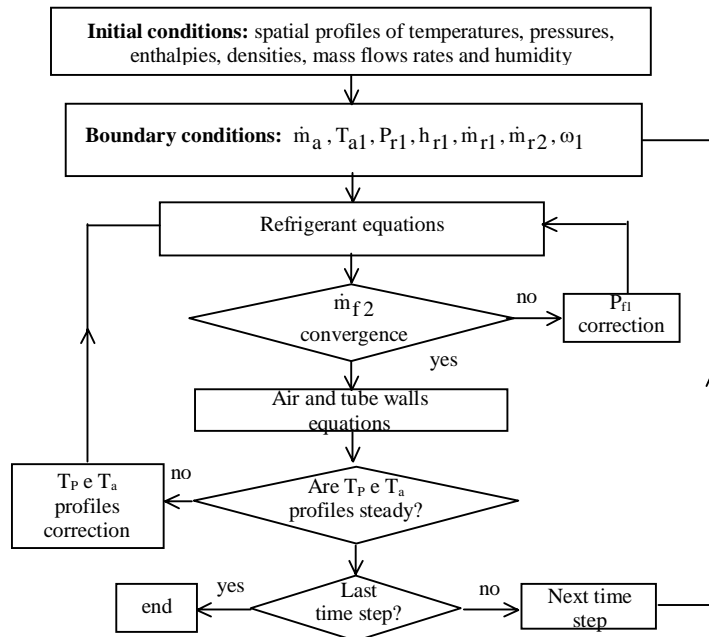


Figure 4. Fluxgram of the model

Since ω_2 depend on tube wall temperature, T_p , an iterative procedure is necessary. Thus, from a guess to T_p , ω_p is calculated, and from these results, ω_2 is obtained. ω_2 is then used to calculate T_p and T_a , and T_p obtained is compared to the guessed T_p . If they are not equal, the iterative procedure is repeated with the new T_p until they converge. The mass transfer coefficient is obtained through heat and mass transfer analogy (Stoecker, 1985).

The chosen correlations to the numerical model are: Hughmark to void fraction, Addoms to heat transfer coefficient in the two-phase zone, Dittus-Boelter in the superheating zone, and a second order polinom in the transition zone. Lockhart-Martinelli to pressure losses and, finally, MacQuiston to heat transfer coefficient from tube to air. The model fluxgram is presented in Fig (4).

4. Simulations with the numerical model

The results obtained with the numerical model can be compared to experimental results from specialized literature. This kind of comparison allows, at the same time, an evaluation of the performance of the model and a demonstration of its versatility in simulations under different conditions. In the next section, experimental data taken from literature is presented. It will be the basis for a comparative study developed in the following sections.

4.1. Comparative study between the refrigerants R22 and R410a

Since the Montreal Protocol on substances that deplete the Ozone layer was signed in September 1987, international efforts have been made in order to find new refrigerants to replace the CFC's and HCFC's. CFC's such R12, were targeted first and their production ceased in 1996 in developed countries. The HCFC's (hydrochlorofluorocarbons) are the next target of the Protocol, which established that the production of these refrigerants must be decreased until its total interruption in 2030.

Several refrigerants have been tested as probable substitutes to R22 and Chin and Spatz (1999), pointed out three candidates: R410a, R407c and R134a. In 1999, Chin and Spatz presented a study comparing R22 and R410a performances. In this study, besides the comparison between the performance coefficients (COP) of an equipment operating with both refrigerants, they collected experimental data referent to the study of heat transfer and pressure losses in phase changing for both refrigerants. These results were presented in graphical form (Fig (5) and (6)).

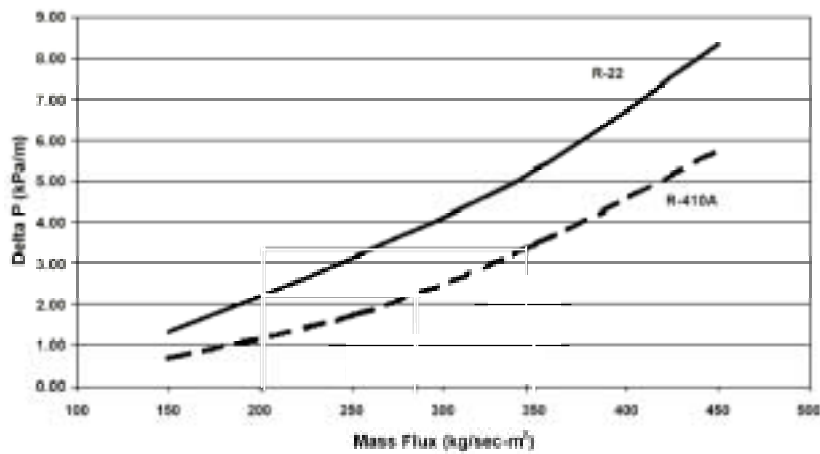


Figure 5. Pressure losses x Mass flux (Chin e Spatz, 1999)

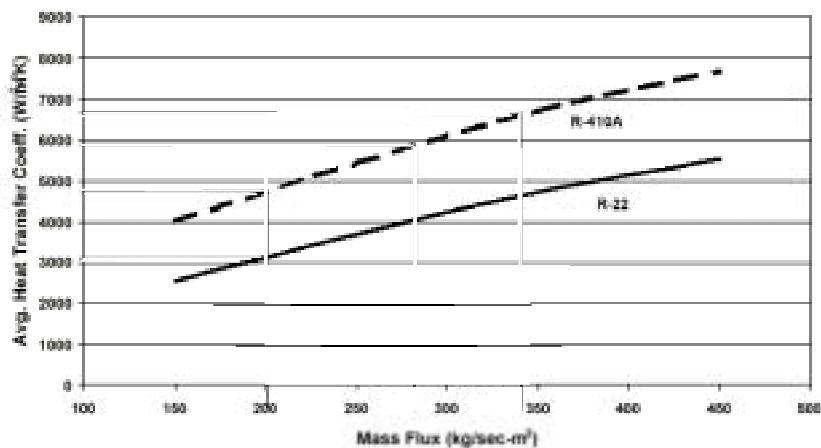


Figure 6. Average heat transfer coefficient x Mass flux (Chin e Spatz, 1999)

The work of Chin and Spatz (1999) showed that the performance of equipment operating with R410a is as good as (if not superior) the performance of the same equipment operating with R22 when working at design conditions. Under temperatures above 40°C, the performance of the equipment operating with R22 is better.

In order to verify the performance of the numerical model, a series of simulations using the refrigerants R22 and R410a were made. Since the work of Chin and Spatz does not bring any information about the kind of air cooler used and the ambient conditions during the experiments, the simulations were realized using the evaporator described in section 3. Thus, the evaporator was divided in 16 control volumes in x-axis, with Δx equal 1.25cm, and in 3 control volumes in y-axis, with Δy equal 2cm. In z-axis, Δz was made equal 1cm resulting in 30 control volumes in this direction. The time step Δt was made equal 5s, the smallest resolution that the model is able to work with. During the simulations, the condensation temperature and subcooling degree were fixed and made equal to both refrigerants while the compressor rotation was varied in order to get different mass velocities. The other input data were dry and wet bulb temperatures of the air, which were, respectively, 24.4°C and 17.2°C, air velocity equal 2.0m/s and mass flow rate equal 27.2kg/h. The results are seen in the Fig (7) and (8).

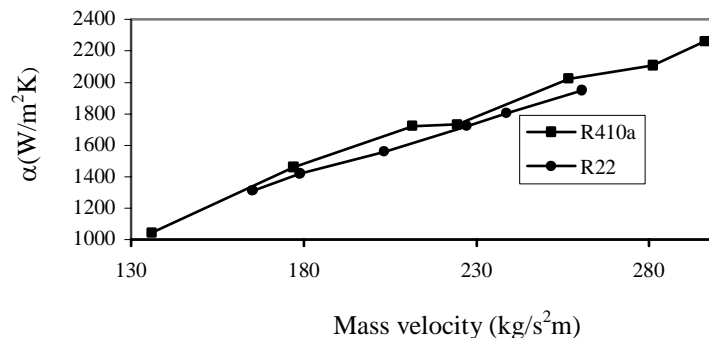


Figure 7. Heat transfer coefficient for R22 and R410a in function of mass velocity

The absence of details about equipment, and its operational conditions, used in the experiments that permitted the construction of the original curves (Fig (5) and (6)), does not permit the adaptation of the model to work under the same conditions for which those points were obtained. Thus, even when the mass velocities are equal, the numerical values obtained by the model cannot be compared to that showed by Chin and Spatz. What can be said, and it is observed, is that the results presented in Fig (7) and (8) confirm the tendencies presented in the work by Chin and Spatz. For the same mass velocity, the pressure losses are smaller to R410 (Fig (6) and (8)) and the opposite is verified to the heat transfer coefficient (Fig (5) and (7)).

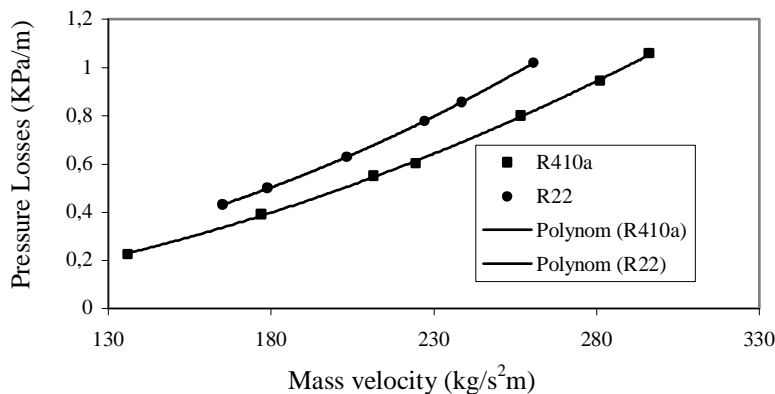


Figure 8. Pressure losses to R22 e to R410a in function of mass velocity

4.2. Simulations with R22 under dynamic conditions

The R22, in spite of being a HCFC, stills being the most used refrigerant in air-conditioning applications in Brazil. Thus, simulations with R22 are more convenient to analyze the thermal behavior of an air cooler operating under dynamic conditions.

During the simulations under dynamic conditions, the compressor and expansion device numerical models were attached to the air cooler model. The Eq. (9) represents the compressor model (Koury, 1998).

$$\dot{m}_c = N \cdot V \cdot \rho_f \cdot \eta \quad (9)$$

Where \dot{m}_c is the mass flow rate imposed by the compressor, N is the rotation in rpm, V is the cylinder volume in m^3 and η_v is the volumetric efficiency of the compressor, and ρ_f is the inlet refrigerant density. The compressor volumetric efficiency is calculated by Eq. (10) (Koury, 1998).

$$\eta_v = 1 + c - c \cdot \left(\frac{P_{\text{cond}}}{P_{\text{eb}}} \right)^{\frac{c_p}{c_v}} \quad (10)$$

Where c is the clearance factor, P_{cond} and P_{eb} are the condensation and ebullition pressures, and c_v and c_p are the inlet refrigerant specific heats at constant volume and pressure, respectively.

For these simulations, the expansion device was considered as fixed orifice kind and the Eq. (11) represents its model.

$$\dot{m}_{\text{ed}} = K_{\text{ed}} \sqrt{\Delta P \cdot \rho_{r4}} \quad (11)$$

Where \dot{m}_{ed} is the mass flow rate in the expansion device, K_{ed} is the expansion device characteristic constant, ΔP is the difference between condensation and ebullition pressures and ρ_{r4} is the refrigerant inlet density.

The Tab. (1) shows the input data used in the numerical model during the simulations. The input data related to air are the same used in the previous section simulations. The expansion device characteristic constant, K_{ed} , was obtained from a steady-state simulation using R22. In this simulation, the compressor and expansion device mass flow rates were equal and, from the operation point obtained, the K_{ed} was calculated.

Table 1. Numerical model input data.

Rotation	500rpm
Cylinder volume	$50 \times 10^{-6} m^3$
C	0.07
T_{cond}	50°C
T_{subcooling}	45°C
K_{ed}	2.053×10^{-7}
m_{R22}	95g

The Fig (9) and (10) show the obtained result for a simulation under dynamic conditions. In these figures, the average outlet air temperature, R22 saturation temperature, superheating degree, compressor and expansion device mass flow rates, and the mass of R22 in the air cooler are plotted in function of time.

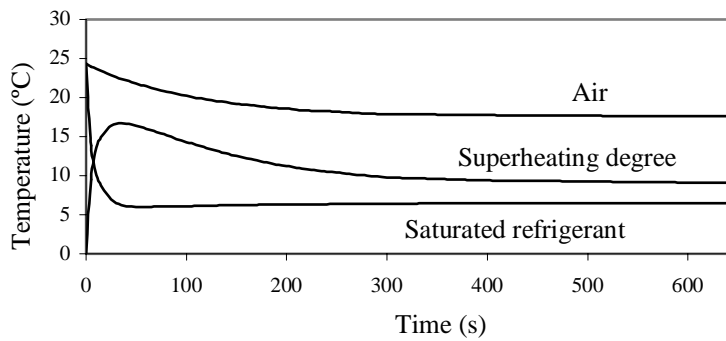


Figure 9. Average outlet air temperature, superheating degree, and refrigerant saturation temperature in function of time.

For this simulation, the air cooler was loaded with an excess of refrigerant mass. After that, the compressor was started up in order to study the dynamic behavior of all the expansion device, compressor and evaporator. In Fig. (10), it might be observed that just at the start up the compressor removes a large amount of refrigerant from the air cooler, while the expansion device stills operating below the steady-state mass flow rate. So that, refrigerant is being removed from the evaporator, which results in an abrupt decrease of the saturation pressure. This might be verified by the decreasing of the saturation temperature during this time interval. This sudden decreasing of mass in evaporator also results in an expressive increasing in the superheating degree.

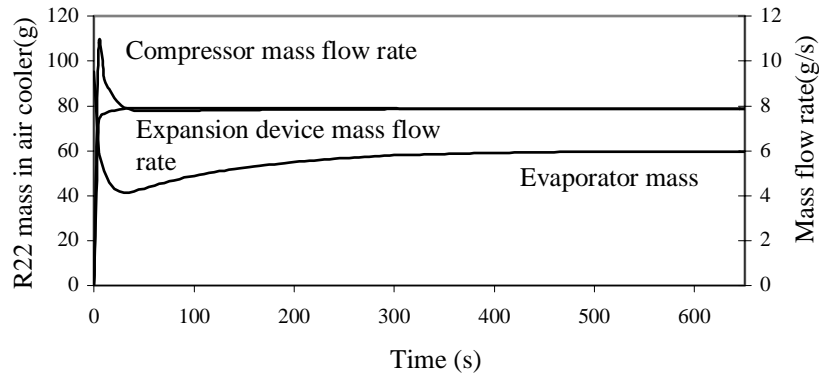


Figure 10. Evaporator mass, expansion device and compressor mass flow rate in function of time

Once the compressor mass flow rate reaches a peak around 5s, it starts to decrease, while the expansion device mass flow rate stills increasing. Since the compressor mass flow rate is bigger yet, mass stills being removed from the evaporator and the refrigerant temperature stills decreasing. The opposite effect is observed in the superheating degree. Around 30s, the mass flow rates are equal and, during a time interval, the mass flow rate in the expansion device is bigger than in the compressor. Thus, the air cooler receives a mass addition, which implies a pressure increasing and, consequently, a saturation temperature increasing. Finally, around 600s, these mass flow rates are equal and, after 200s approximately, the evaporator starts to work under steady-state conditions, with definite mass and temperatures (Fig (11) and (12)).

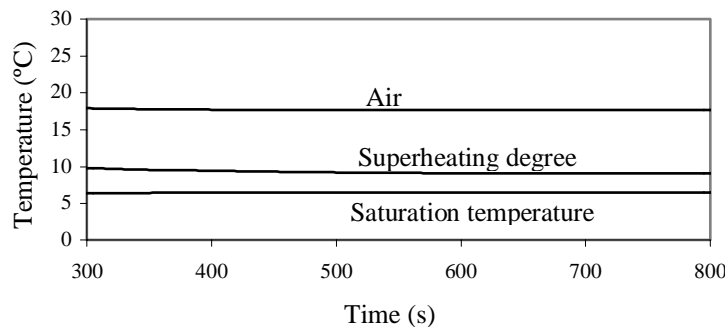


Figure 11. Average outlet air temperature, superheating degree, and refrigerant saturation temperature in function of time (zoom in scale)

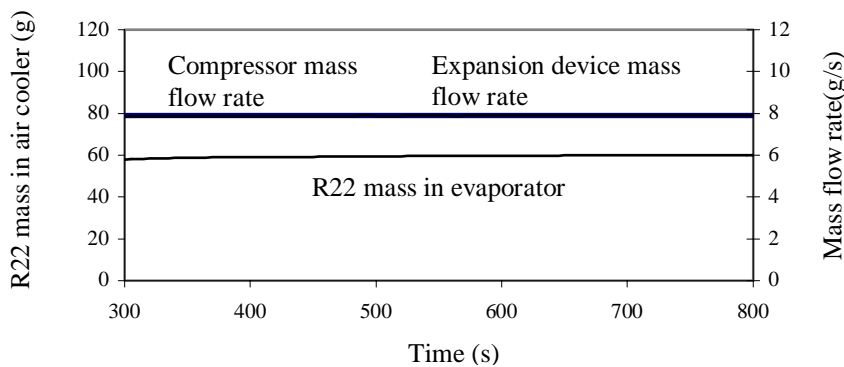


Figure 12. Evaporator mass, expansion device and compressor mass flow rate in function of time (zoom in scale)

6. Conclusion

The purpose of this work was the development of a numerical model of an air cooler working under dynamic conditions. The numerical model developed allows the realization of simulations using different geometries for the evaporator – which is important because this kind of heat exchanger is found in a wide variety of geometries – and also different refrigerants, which is very important in times when many refrigerants have been tested in order to substitute that contributes to the ozone layer depletion. Theoretical data obtained by model simulations working with R22 and R410a refrigerants, repeated tendencies observed in experimental data taken from literature.

7. References

- Chin, L., Spatz, M.W., 1999, *Issues relating to the adoption of R-410a in air conditioning systems*. 20th International Congress of Refrigeration, IIR/IIF, Sydney, Volume II, paper 179.
- Cleland, A. C., 1986, *Computer subroutines for rapid evaluation of refrigerant thermodynamic properties*. Int. J. Refrig., november, Vol. 9, p. 329-335.
- Jia, X., Tso, C.P., Chia, P.K., Jolly, P. 1995, *A distributed model for prediction of the transient response of an evaporator*. Int. J. Refrig, Vol. 18, Nº 5, p. 336-342.
- Koury, R. N. N., 1998. *Modelagem numérica de uma máquina frigorífica de compressão de vapor*. Campinas: Universidade Estadual de Campinas, 112 p. (Tese, Doutorado em Engenharia Mecânica).
- Liang, S.Y., Wong, T.N., Nathan, G.K., 2001, *Numerical and experimental studies of refrigerant circuitry of evaporator coils*. Int. J. Refrig., Vol 24, p. 823-833.
- Macarthur, J.W., Grald, E.W. 1989, *Unsteady compressible two-phase flow model for predicting cyclic heat pump performance and a comparison with experimental data*. Int. J. Refrig., p. 29-41.
- Machado, L., 1996, *Modele de simulation et etude experimentale d'un evaporateur de machine frigorifique en regime transitoire*. Lyon: L'Institute National des Sciences Appliquees de Lyon, 160p. (Tese, Doutorado em Engenharia Térmica e Energética)
- McQuiston, F., 1981, *Finned tube heat exchangers: state of the art for the air side*. ASHRAE Transaction, p. 1077-1085.
- Stoecker, W.F., Jones, W.J. 1985, *Refrigeração e ar condicionado*. 1.ed. São Paulo: McGraw-Hill do Brasil, 481p.
- Wang, H., Toubert, S. *Distributed and non-steady-state modelling of an air cooler*. 1991, Int. J. Refrig., Vol 14, p. 98-111.